Study of Neutral Final States in K^-p Interactions at Center-of-Mass Energies from 1580 to 1720 MeV*

T. Dombeck†
Argonne National Laboratory, Argonne, Illinois 60439
and Northwestern University, Evanston, Illinois 60201

and

W. W. M. Allison,‡ J. Campbell, Y. Cho, M. Derrick,
R. Engelmann, T. Groves, T. P. Wangler, and N. S. Wong§
Argonne National Laboratory, Argonne, Illinois 60439

and

D. Koetke
Concordia College, River Forest, Illinois 60305
(Received 5 June 1972)

The results reported in this paper come from a K^-p-formation experiment performed in the Argonne-Michigan 40-in. heavy-liquid bubble chamber. About 500 000 pictures were taken in a mixture of 80% propane (C_3H_8) and 20% Freon (CF_3Br) with K^- beam momenta between 730 and 900 MeV/c. Cross sections for the pure isospin states $\Sigma^0\pi^0$, $\Lambda^0\pi^0\pi^0$, and $\Sigma^0\pi^0\pi^0$ in the center-of-mass energy ranging from 1580 to 1720 MeV were measured. Cross-section measurements of the $\Lambda^0\pi^0$, $\Lambda^0\eta^0$, $\Lambda^0\pi^+\pi^-$, and $\Sigma^0\pi^+\pi^-$ final states were compared with previous data obtained using hydrogen bubble chambers to check the validity of our techniques. The cross-section normalization was performed using τ decays to determine the kaon flux. The angular distributions for $\Lambda^0\pi^0$ and $\Sigma^0\pi^0$ are also presented and compared with previous measurements in hydrogen bubble chambers. A check of the technique used previously in hydrogen-bubble-chamber experiments to obtain the $\Sigma^0\pi^0$ angular distributions suggests some contamination in the hydrogen data from the multiple π^0 final states. Our data are consistent with the $\Lambda^0\pi^0\pi^0$ final state being produced almost entirely through $\Sigma(1385)\pi$, and the $\Sigma^0\pi^0\pi^0$ data with almost total $\Lambda(1405)\pi$ production.

I. INTRODUCTION

We report on a low-energy K^-p formation experiment performed in a heavy-liquid bubble chamber in order to investigate the final states:

$$K^-p \to \Lambda^0\pi^0 \quad (I=1), \quad \text{(a)}$$
$$\Lambda^0\eta^0 \quad (I=0), \quad \text{(b)}$$
$$\Sigma^0\pi^0 \quad (I=0), \quad \text{(c)}$$
$$\Lambda^0\pi^0\pi^0 \quad (I=0), \quad \text{(d)}$$
$$\Sigma^0\pi^0\pi^0 \quad (I=1). \quad \text{(e)}$$

As indicated, each of these neutral states has a pure isospin, and the information obtained from them is complementary to that obtained from the charged final states which have been extensively studied in the same energy region.[1-8]

There is information available on reactions (a), (b), and (c) with $\Lambda^0\pi^0$ and $\Lambda^0\eta^0$ final states having been studied in detail. Therefore, we use these two reactions along with a sample of $\Lambda^0\pi^+\pi^-$ and $\Sigma^0\pi^+\pi^-$ events as a test of our techniques. The $\Sigma^0\pi^0$ final state has been studied in hydrogen bubble chambers by selecting a particular region of the missing mass from the Λ^0. Since we detect the γ rays, we provide a new measurement of this final state. The three-body reactions (d) and (e) cannot be observed without γ-ray detection, so that only an upper limit on their combined cross sections is available. Thus, this experiment represents the first study of these reactions in this energy range.

The experimental details are given in Sec. II, and the background determination is discussed in Sec. III. Section IV presents our results, and Sec. V contains the summary and conclusions. We present cross sections for reactions (a)–(e) and the $\Lambda^0\pi^0$ and $\Sigma^0\pi^0$ center-of-mass angular distributions for different momentum regions to compare them with the previous measurements. For $\Sigma^0\pi^0$, we discuss the possibility of contamination in the hydrogen data from the multiple π^0 final states because the γ rays were not detected. In the $\Lambda^0\pi^0\pi^0$ and $\Sigma^0\pi^0\pi^0$ final states, we look for evidence of intermediate states of $\Sigma(1385)\pi$ and $\Lambda(1405)\pi$.

II. EXPERIMENTAL DETAILS

A. Exposure

The experiment was based on an analysis of 487 000 pictures taken in the Argonne-Michigan 40-in. heavy-liquid bubble chamber.[9] The magnetic field in the chamber was 46 kG. The chamber was filled with a mixture of 80% propane (C_3H_8) and 20% Freon (CF_3Br) by volume, and was exposed to a flux of negative kaons at the 28° beam of the ZGS.[10] Table I summarizes the properties of this mixture under the operating conditions of the chamber. The choice of the 80-20 mixture maximized the $\Sigma^0\pi^0$ yield when both two and three γ-ray events were used.

The pictures were taken at the four beam momentum settings of approximately 735, 785, 835, and 860 MeV/c at the entrance to the fiducial region. The optics of the magnetic channel produced a spread of about ±1% in the kaon momentum at the chamber window. However, the momentum of the particles was spread further by momentum loss in the liquid which for minimally ionizing particles was 1.5 MeV/c per cm. This resulted in a kaon momentum variation across the fiducial region of about 150 MeV/c for each beam momentum setting.

B. Scanning and Measuring

The event topology that was the central investigation of this experiment[11] had a kaon interacting giving no charged prongs but with a visible Vee and with any number of γ-ray conversions. A γ-ray conversion was defined to be either an internal or external electron-positron pair, or a single electron or positron track arising from either Compton collisions or asymmetric e^+e^- pairs. Other topologies that were found in the scanning included (1) three-prong events with no visible recoils, (2) two-prong events with a Vee, no visible recoils and any number of γ conversions, (3) events with one negative prong, no visible recoils and any number of γ conversions, and (4) one-prong events with a Vee, no visible recoil and any number of γ conversions. τ decays and $K_{\pi 2}$ decays were obtained from events in categories (1) and (3), respectively. Category (2) contained the $\Lambda^0\pi^+\pi^-$ and $\Sigma^0\pi^+\pi^-$ events produced off hydrogen. Events in category (4) were used in a study of the background.

About 75% of the film was double-scanned and the results were edited by a third scanner who was instructed not only to check the discrepancies resulting from the initial scans, but also to look a third time for converted γ rays. On the remainder of the film, only a single scan was performed, and a scan edit constituted a second scan for converted γ rays. The scanning efficiencies for detecting a zero-prong-plus-Vee interaction with any number of γ rays were determined to be 96% and 76%, respectively, for the samples that were double- and single-scanned.

The events were hand-measured using both image and film plane digitizers. Individual tracks which failed geometrical reconstruction were remeasured once and used with the previously reconstructed values of the other tracks in the event. Even so, 7% of all the zero-prong events with γ rays failed to reconstruct and an appropriate correction was made for them in computing cross sections.

C. Geometry and Kinematics

The events were reconstructed in space and geometry errors assigned using the program SHAPE.[12] A correction for radiation losses on electron

TABLE I. Properties of the 80% propane (C_3H_8)-20% Freon (CF_3Br) mixture.

Density	0.6435 g cm^{-3}
Radiation length	39 cm
Average γ conversion length	55 cm
Kaon interaction length at 700 GeV/c	171 cm
Partial density of hydrogen	0.0625 g cm^{-3}
Partial density of carbon	0.305 g cm^{-3}
Partial density of fluorine	0.115 g cm^{-3}
Partial density of bromine	0.161 g cm^{-3}
Percent of kaon interactions[a] with	
Free hydrogen	24%
Carbon	46%
Fluorine	16%
Bromine	14%

[a]Assuming that cross sections off heavy nuclei are $A^{2/3}$ of the K^- cross section.

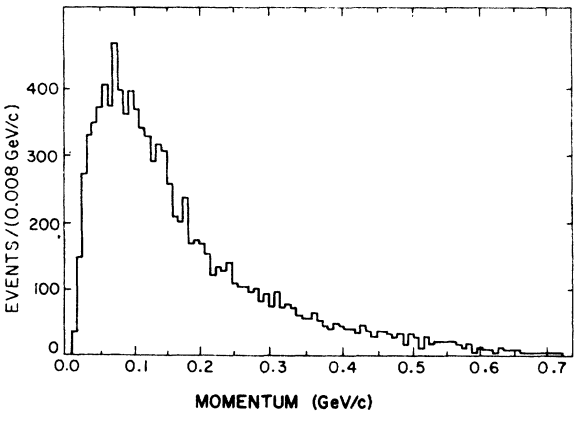

FIG. 1. γ-ray momentum distribution for 10 244 γ rays.

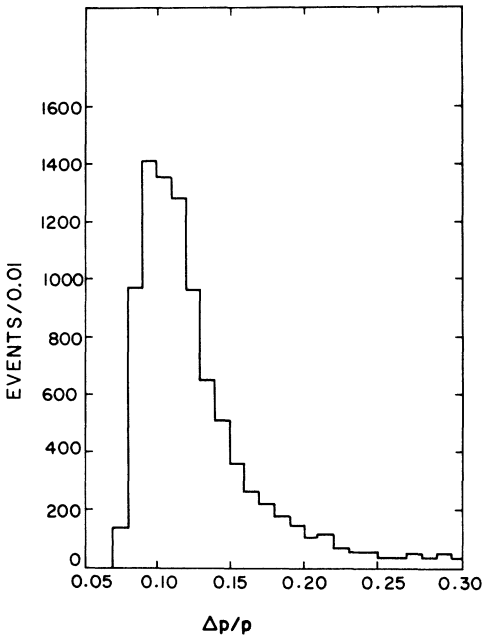

FIG. 2. γ-ray fractional momentum errors.

tracks was made using the Behr-Mittner method.[13,14] SHAPE reconstructed the γ-ray momenta and errors from the measured electrons. The distributions of the γ-ray momenta and percent errors are shown in Figs. 1 and 2. The mean momentum was 150 MeV/c and the mean $\Delta p/p$ was 12%.

The radiative energy loss constant for electrons was set using the γ-γ effective-mass combinations

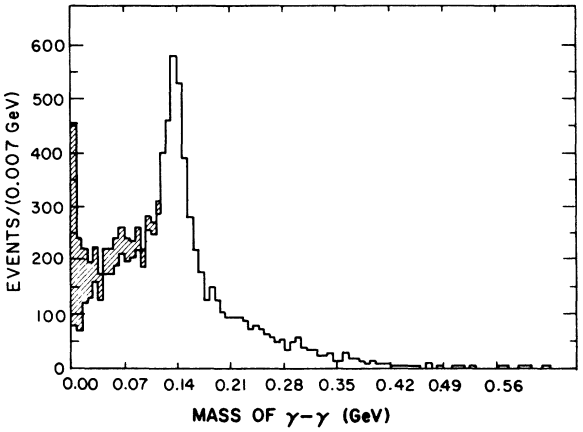

FIG. 3. The γ-γ effective-mass combinations. The cross-hatched events have bremsstrahlung daughters.

from the geometry data to give the best π^0 mass distribution as shown in Fig. 3. For the final value of the correction constant, the π^0 signal was very prominent and centered on the correct mass. The full width at half maximum of the observed π^0 signal was 28 MeV. The η^0 was expected to have an observed width of 140 MeV, so that detection of an η^0 signal at 549 MeV would be difficult.

The γ-ray angles were determined in two ways: (1) from the K^- interaction vertex and the γ-ray conversion point and (2) from the electron directions. A γ-ray pointing test was provided by comparing these two determinations of the angles. This test was used to eliminate nonpointing γ rays for

TABLE II. Kinematic fits and constraint classes attempted in GRIND.

Topology	No. of γ's	Fits attempted[a]	No. of constraints[b]
0-prong + Vee	2	$K^-p \to \Sigma^0\pi^0$	3
		$\Lambda^0\pi^0$	5
		$\Lambda^0\eta^0$	5
	3	$K^-p \to \Lambda^0\pi^0\pi^0$	3
		$\Sigma^0\pi^0$	6
	4	$K^-p \to \Sigma^0\pi^0\pi^0$	4
		$\Lambda^0\pi^0\pi^0$	6
2-prong + Vee	0	$K^-p \to \Lambda^0\pi^+\pi^-$	4
	1	$K^-p \to \Sigma^0\pi^+\pi^-$	5
1-prong, no Vee	1	$K^- \to \pi^-\pi^0$	2
	2	$K^- \to \pi^-\pi^0$	5
3-prong	0	$K^- \to \pi^+\pi^-\pi^-$	4

[a]A fit was tried for each permutation of the measured γ rays. Also, all combinations were tried assuming a missing γ ray as well. All lower fits were attempted by systematically throwing out γ rays. Fits using a missing π^0 were also attempted.

[b]These include kinematic plus mass constraints minus the missing quantities.

the lower constraint fits. A bremsstrahlung test was performed on each γ ray to determine if it might have originated from another γ ray in the event. A γ ray was called a bremsstrahlung daughter if it fell within four standard deviations of pointing in the same direction as a γ ray closer to the interaction vertex. γ rays satisfying this test were removed from the final sample and the momentum error of the parent γ ray was increased to account for the energy lost in the bremsstrahlung. This bremsstrahlung is evident in Fig. 3 as a peak at zero mass. Making the above bremsstrahlung cut removed the cross-hatched events.

The kinematic constraint program GRIND[15] attempted various hypotheses for each measured topology as listed in Table II. In order to study ambiguities and backgrounds, all possible lower-constraint fits were tried for each event by systematically removing each γ, one at a time. The resolution of these ambiguities is discussed later.

D. Corrections for Event Losses

Events were lost or dropped to lower constraint classes since not all γ rays converted in the chamber. In addition, events were lost when a Λ decayed near the kaon interaction point. A 20% correction was made for this loss using the measured Λ^0 lifetime.[16] Smaller corrections deduced from an observed anisotropy in the Λ^0 decay distribution (7%) and Λ^0 interactions in the chamber liquid (1.5%) were also applied to the data.

Because of the limited flight path available, 48% of the γ rays did not convert in the chamber. The geometrical correction was made using a conversion length computed as a function of momentum for each γ ray.[17,18] Added to this geometrical loss were the γ-ray scanning inefficiencies caused by a number of effects, the most important being (1) e^+-e^- pairs having small projected momentum in a plane perpendicular to the magnetic field, and (2) Compton electrons or e^+-e^- pairs with very asymmetric energy sharing between the electrons.

The loss of γ rays due to small projected momentum for the e^+-e^- pair was observed by a lack of azimuthal isotropy of the γ rays about the beam direction. Because of the expected isotropy, the momentum distribution projected onto the plane perpendicular to the magnetic field should have been the same as that projected into the plane parallel to the magnetic field. A direct comparison of these two distributions yielded the scanning efficiency as a function of projected momentum shown in Fig. 4. Above 100 MeV/c in projected momentum, the detection efficiency was high, and it dropped sharply below this value. Overall, the average correction for this effect amounted to 13% per γ ray.

Comparison of observed γ rays with a prediction for energy sharing between electron and positron[19] showed a loss of very asymmetric pairs. The computed efficiency data are shown as a function of γ-ray momentum in Fig. 5. The falloff with increasing momentum was believed to be due to the single electron track appearing straight rather than as the more characteristic spiral. This loss of asymmetric γ rays amounted to an average correction of 4% per γ ray.

Using the double-scan information and isolating only γ rays with projected momenta greater than 100 MeV/c and symmetric energy sharing between the electrons, a scanning efficiency of $(95 \pm 5)\%$ was computed and applied to all the γ rays in the final sample. Therefore, multiplying together the three major γ-ray inefficiencies yielded an average efficiency of $0.87 \times 0.96 \times 0.95 = 0.79$ with a com-

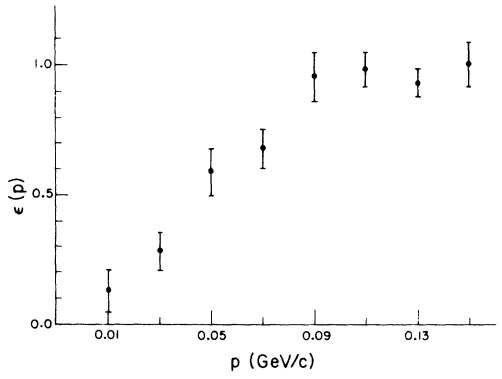

FIG. 4. γ-ray scanning efficiency as a function of projected momentum.

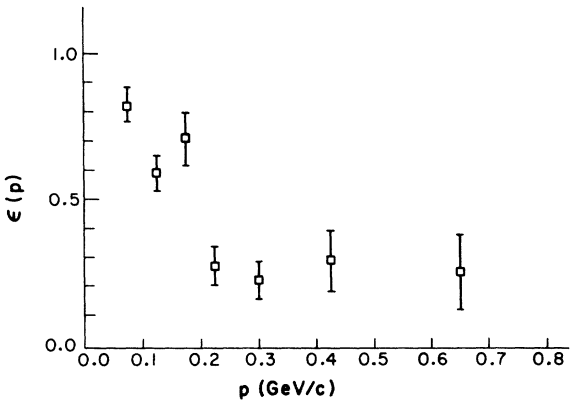

FIG. 5. The efficiency for detecting one-prong γ conversions, consisting of both asymmetric pairs and Comptons, as a function of momentum.

puted error of ±0.09. However, using all the γ rays found in the scanning, an over-all scanning efficiency of 0.96 ± 0.02 was computed. It appears then that the experiment produced a class of γ rays with small projected momentum and asymmetric energy sharing which were found with zero efficiency by all scanners.

E. Flux Determination

Of the three-prong events, which were scanned over the entire sample of film, about one-half were measured and fitted. Background from three-prong interactions off heavy nuclei was very small as seen in the missing mass plot of Fig. 6. The resulting beam momentum distribution is shown in Fig. 7. The distribution peaks near 750 MeV/c and has a usable range from 540 to 860 MeV/c. The absolute kaon flux and, therefore, the cross-section normalization was determined using τ decays. This method properly handled the problems arising from attenuation in the beam due to decays and interactions across the fiducial volume.

A small sample of events, representing the $K_{\pi 2}$ decay mode, was used as a consistency check for the techniques devised to handle the γ-ray losses and provided an independent flux determination. For the $K_{\pi 2}$ events, in which both γ rays converted, Fig. 8 shows the $\gamma\gamma$ mass plotted against the $\pi^-\gamma\gamma$ mass. A clear signal is seen and after removal of the fitted events, a small background remains. A similar check was done for the single-γ $K_{\pi 2}$ events. The resulting ratio of $K_{\pi 2}$ to τ decays was in agreement with the accepted value within the error.

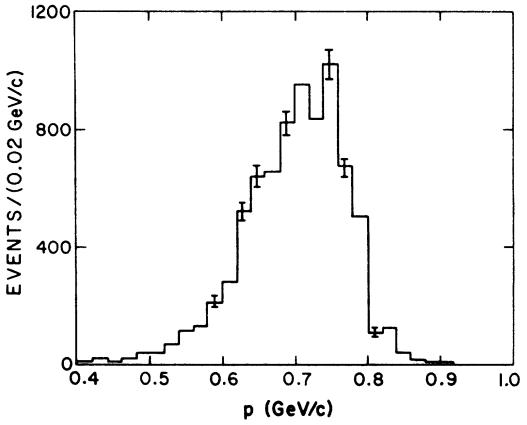

FIG. 7. Beam-momentum distribution from the measured τ-decay fits.

III. BACKGROUND DETERMINATION

A. Sources of Background

The hydrogen signal is shown in Fig. 9 where we have plotted the missing mass squared off the Λ versus the effective mass of the two γ rays. We expect the hydrogen events of $K^-p \to \Lambda^0\pi^0$ to give a

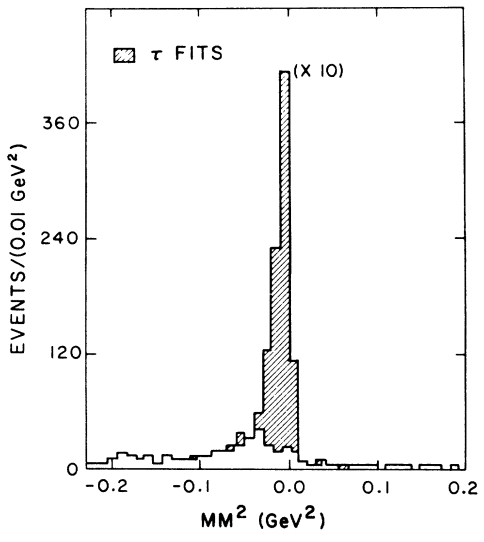

FIG. 6. Missing mass squared off the beam and three outgoing pions for the 5084 three-prong events. The cross-hatched events made 4C fits to the τ decays. The bin at zero missing mass squared has been displayed at a reduction by a factor of 10.

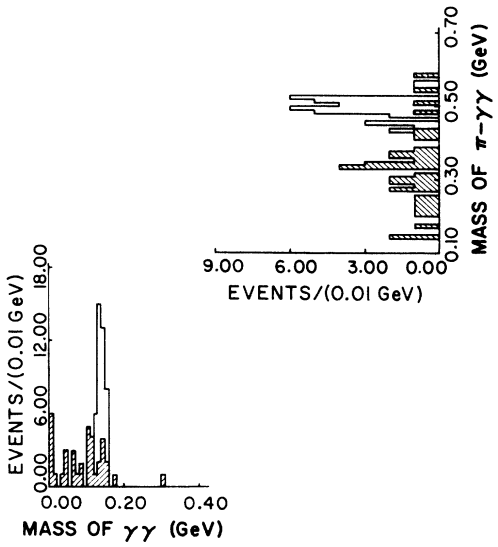

FIG. 8. Mass of $\gamma\gamma$ versus mass of $\pi^-\gamma\gamma$ for one-prong events with two γ's and with the missing mass cut of $-0.02 \leq \mathrm{MM}^2(\pi^-\gamma\gamma) \leq 0.02$ GeV^2. The cross-hatched events did not fit the $K_{\pi 2}$ hypothesis.

simultaneous signal at 0.2 GeV^2 in missing mass squared and 0.135 GeV in effective mass. It is evident that the background beneath the signal on this plot is large.

In addition to the lack of complete γ-ray conversion, the sample of events found in the scanning was also contaminated by interactions on bound nucleons. After removing events with obvious stubs at the production vertex, the 3 : 1 bound-nucleon- to free-nucleon-event ratio listed in Table I was reduced to about 1.5 : 1. The two major sources of contamination in the fits were (i) events originating off heavy nuclei and (ii) hydrogen events that fed into lower constraint classes because not all the γ rays converted. We called this latter class of events the "γ-deficient" background. As an example, a four-γ $\Lambda^0\pi^0\pi^0$ event, for which only two γ rays were detected, could give a $\Lambda^0\pi^0$ (2γ) fit because of measurement errors and so be misidentified.

B. The "Pseudoevent" Method

There are many reactions that might occur off the bound protons or neutrons in the nuclei and yield hydrogenlike events. The situation is complicated by the possibility of secondary scatters occurring in the nucleus. In order to study this problem, a sample of one-prong-plus-Vee events was isolated, because these events could only occur off heavy nuclei. In the final sample, the ratio of positive one-prong events to negative one-prong events was 2 : 3, indicating that secondary interactions are important.

The sample of one-prong events was measured and after geometrical reconstruction, the charged pions (both positive and negative) were assumed to be π^0's and allowed to decay into two γ rays in a Monte Carlo simulation. The γ-ray parameters were smeared according to the observed errors in the experiment and randomly tagged as having been detected or undetected according to the various detection efficiencies. These simulated γ rays were added to those already measured in the event. The number of measured one-prong events was 748, yielding 172, 56, and 17 events with two, three, and four γ rays, respectively. These events, which we call "pseudoevents," were processed in GRIND just like the real zero-prong events.

It is assumed that the pseudoevents making fits represent in some approximation the zero-prong nuclear events. There is no theoretical justification that this is true, and we will argue from purely empirical grounds. Whenever possible, we use the pseudoevents to indicate the appropriate χ^2 probability cutoff to apply to the fits in order to isolate a clean sample of events. Only the events restricted by the χ^2 cut are used for angular distributions, etc. For cross-section purposes, the errors are increased in order to take into account our uncertainty about the distribution of nuclear events and real hydrogen events below the χ^2 cutoff.

In Fig. 10, the two-γ pseudoevent scatter plot is

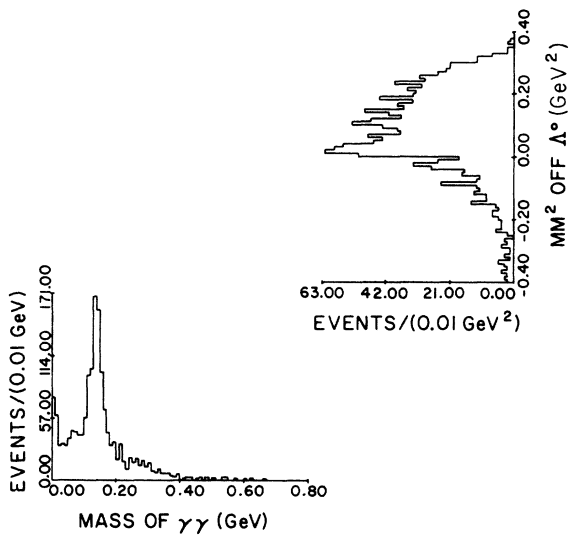

FIG. 9. Mass of $\gamma\gamma$ versus missing mass squared off Λ^0 for zero-prong-plus-Vee and 2γ events.

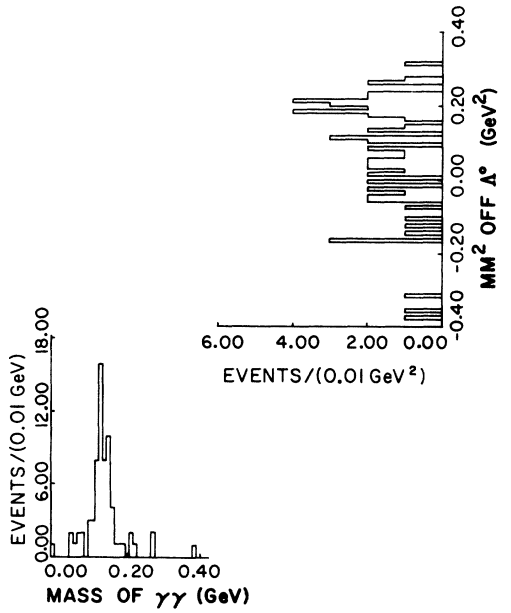

FIG. 10. Mass of $\gamma\gamma$ versus missing mass squared off Λ^0 for 2γ pseudoevents.

shown, which corresponds to Fig. 9 for the real events. The projection from Fig. 9 is replotted in Fig. 11 where a Monte Carlo calculation has been used to predict the hydrogen signal in this plot, assuming phase-space distributions for $\Lambda^0\pi^0\pi^0$ and $\Sigma^0\pi^0\pi^0$. We have subtracted all two-γ combinations predicted to contribute to this plot from the hydrogen final states $\Sigma^0\pi^0\pi^0$, $\Lambda^0\pi^0\pi^0$, $\Sigma^0\pi^0$, and $\Lambda^0\pi^0$, and the cross-hatched events remain after the Monte Carlo hydrogen subtraction. Thus, we are able to estimate the nuclear background level in the real zero-prong events. The points plotted in Fig. 11 were taken from the projection of the pseudoevents in Fig. 10, normalized to yield equal areas beneath both histograms. In general, agreement is very good and consistent with the pseudoevents distributing in the same manner as the background. The normalization factor for the two-γ pseudoevents was 16.3 ± 2.1. This factor was applied to both the $\Lambda^0\pi^0$ and $\Sigma^0\pi^0$ (2γ) pseudoevent fits to yield a quantitative estimate for the background predicted in each final state. In the same manner, background predictions were made for the other final states. In each case, agreement was observed between the pseudoevents and the background level after substracting the Monte Carlo results for the hydrogen events.[11]

C. γ-Deficient Events

The highest-constraint fits provided an accurate means by which to study the problem of ambiguous fits and multi-γ-ray events feeding the lower final states. For example, we took an event having its full compliment of γ rays that made a fit to $\Lambda^0\pi^0\pi^0$ or $\Sigma^0\pi^0\pi^0$ and asked how often it also fit $\Sigma^0\pi^0$ or $\Lambda^0\pi^0$ when the γ rays were systematically removed. Knowing the number of such fits, the resulting background due to this effect was obtained for each final state. It was hypothesized that the pseudoevents contained multi-γ-ray events produced off heavy nuclei which might appear as hydrogen events. Using the higher-constraint fits, we were able to resolve all the lower-constraint ambiguities and make subtractions in the data whenever necessary. The study of this type of background revealed that fits with a missing π^0 were not usable.

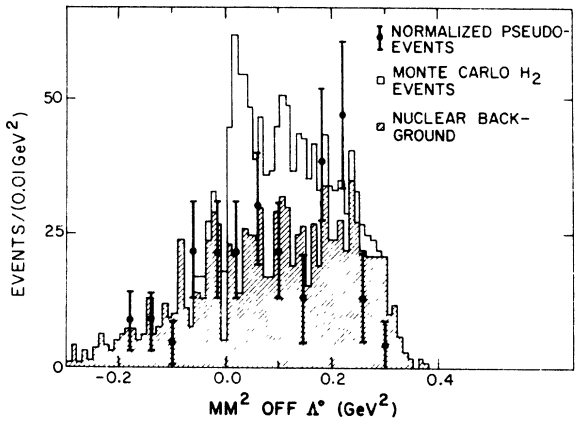

FIG. 11. Missing mass squared off Λ^0. The 2γ hydrogen events predicted from a Monte Carlo program have been subtracted, leaving the cross-hatched region. The data points are the pseudoevents.

D. Selection of Hydrogen Fits

A peak at χ^2 probabilities below about $p(\chi^2) = 0.05$ is generally observed for each sample of fitted events and is believed to be due to a combination of genuine signal events with non-Gaussian track errors, and background events, arising from nuclear interactions or events with undetected γ rays. A general procedure was applied to each final state in order to isolate a pure sample of events for angular distribution studies and also to produce the best cross-section measurements. A test of the method is the comparison of the $\Lambda^0\pi^0$ cross section as measured in this experiment with previous measurements in hydrogen, as discussed in Sec. IV.

The χ^2 probability distributions for each final state, after subtracting the pseudoevent and γ-deficient event background, revealed that a minimum value of $p(\chi^2) = 10^{-6}$ included the entire sample of signal events. General cuts were made on this sample to eliminate fits that used nonpointing and bremsstrahlung γ rays. The resulting sample of fitted events for each final state is listed in the first column of Table III.

TABLE III. Number of fits.

Final state	Surviving general cuts	Surviving χ^2 cut[a]
$\Lambda^0\pi^+\pi^-$ [b]	393	393
$\Sigma^0\pi^+\pi^-$ (1γ) [c,b]	30	30
$\Lambda^0\eta^0$ (2γ) [d]	16	16
$\Lambda^0\pi^0$ (2γ) [d]	192	119
$\Sigma^0\pi^0$ (2γ) [c,d]	247	157
$\Sigma^0\pi^0$ (3γ) [c]	164	133
$\Lambda^0\pi^0\pi^0$ (3γ)	332	276
$\Lambda^0\pi^0\pi^0$ (4γ)	25	20
$\Sigma^0\pi^0\pi^0$ (4γ) [c]	24	24
$\Sigma^0\pi^0\pi^0$ (5γ) [c]	3	3

[a] Fits used in the angular distributions, etc.
[b] Events scanned only on 17% of the total sample.
[c] Only fits having a Σ^0 using a measured γ ray are given.
[d] Events scanned only on 34% of the total sample.

TABLE IV. Summary of the background analysis.

Final state	χ^2 probability cutoff	Nuclear background[a]	γ-deficient fits background[a]	Correction for events below χ^2 cutoff
$\Lambda^0\pi^+\pi^-$	10^{-6}	(1± 0.5)%	(7± 2)%	•••
$\Sigma^0\pi^+\pi^-$	10^{-6}	(0± 12)%	None	•••
$\Lambda^0\pi^0$	10^{-2}	(0± 14)%	(18± 6)%	(13± 13)%
$\Sigma^0\pi^0$ (2γ)	10^{-2}	(11± 1)%	(6± 3)%	(31± 31)%
$\Sigma^0\pi^0$ (3γ)	10^{-4}	(0± 12)%	(3± 2)%	(15± 15)%
$\Lambda^0\pi^0\pi^0$ (3γ)	10^{-5}	(47± 11)%	(8± 3)%	None
$\Lambda^0\pi^0\pi^0$ (4γ)	10^{-2}	(0± 85)%	(8± 8)%	(14± 14)%
$\Sigma^0\pi^0\pi^0$ (4γ)	10^{-6}	(0± 100)%	None	•••
$\Sigma^0\pi^0\pi^0$ (5γ)	10^{-6}	(0± 100)%	None	•••

[a]This is the background remaining after the χ^2 probability cut has been imposed as determined from the pseudoevent sample.

[b]We assume that the best estimate of the background is 0.0 with a statistical error assigned corresponding to 1 event.

In order to isolate a subsample of events of high purity for angular distributions, we imposed a χ^2 probability cut which depended upon the predicted background for each final state. The number of events surviving the χ^2 cut are shown in the second column of Table III. The values of these probability cuts and the estimates of the background events still remaining, are given in Table IV.

To determine the various cross sections, a correction was made to include real events which were below the χ^2 probability cutoff. We first subtracted the relatively well-determined γ-deficient background from the fitted events below the cutoff. Then, since the nuclear background was less well determined, we assigned the remaining events equally to genuine signal events off hydrogen and to nuclear background events. Large errors were assigned to account for the uncertainty in the procedure as shown in the last column of Table IV. As seen in Table IV, this procedure on occasion resulted in relatively large corrections and associated large errors.

IV. RESULTS

A. Search for the $\Lambda(1327)$

A baryon resonance with a mass near 1327 MeV decaying into $\Lambda^0\gamma$ has been reported in heavy-liquid bubble chamber work performed at Dubna.[20] We have used only our sample of Λ^0 events with three observed γ rays in order to place an upper limit on the cross section for resonant production in the 1327-MeV region. Using the three γ events, we compare the cross section for $\Lambda(1327)\pi^0$ production to $\Sigma^0\pi^0$ production in the same momentum region. In Fig. 12(a), we have plotted the $\Lambda^0\gamma$ effective masses with three $\Lambda^0\gamma$ combinations plotted for every event. We eliminated many of the nuclear events by restricting ourselves to events with $-0.02 \leq \mathrm{MM}^2(\Lambda^0\gamma\gamma\gamma) \leq 0.02$ GeV^2. In order to reduce the combinatorial background, only events for which the mass of the two remaining gammas was near a π^0 were chosen, i.e., $0.10 \leq M(\gamma\gamma) \leq 0.16$ GeV, and these have been plotted in Fig. 12(b). An estimate of the combinatorial background

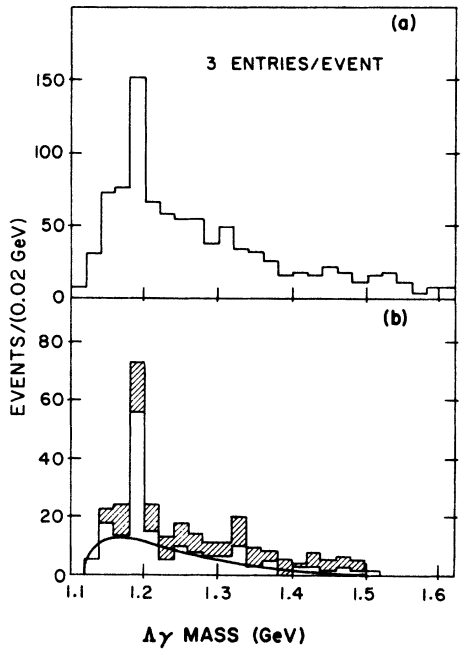

FIG. 12. Mass of $\Lambda^0\gamma$ for 3γ events. Figure 12(a) is for $-0.02 \leq \mathrm{MM}^2(\Lambda^0\gamma\gamma\gamma) \leq 0.02$ GeV^2. Figure 12(b) shows the effect of an additional cut selecting events with the mass of the two remaining γ's of $0.10 \leq M(\gamma_i\,\gamma_j) \leq 0.16$ GeV. The cross-hatched events represent background included in the π^0 region. The curve is explained in the text.

beneath the π^0 region was subtracted out by taking an average of the events in the upper and lower adjoining regions. The resulting background subtraction is shown in Fig. 12(b) as the cross-hatched events.

The events remaining in the $\Lambda^0\gamma$ mass distribution after making the above cuts are due to $\Sigma^0\pi^0$, $\Lambda^0\pi^0\pi^0$, $\Sigma^0\pi^0\pi^0$, and any signal from $\Lambda(1327)\pi^0$. Using a Monte Carlo prediction for the $\Lambda^0\pi^0\pi^0$ and $\Sigma^0\pi^0\pi^0$ final states, we have generated the curve in Fig. 12(b) which was normalized to the data outside of the Σ^0 signal beyond 1.24 GeV. Since there were only six events above this curve in the 1320-MeV region, we ignored the effects of weighting the γ-ray events, and have compared these events with the 52 events above the curve in the Σ^0 region to obtain an upper limit on the cross section of $\sigma(\Lambda(1327)\pi^0) \leq 0.12\ \sigma(\Sigma^0\pi^0)$. Using the average cross sections for $\Sigma^0\pi^0$ production which are discussed later in this section, we computed an upper limit for the average cross section of $\sigma(\Lambda(1327)\pi^0) \leq 340\ \mu$b over the K^- momentum region from 0.56 to 0.86 GeV/c. This result is in agreement with the more stringent limits given by hydrogen and deuterium experiments which have failed to see the $\Lambda(1327)$,[21,22] and also with a recent heavy-liquid chamber experiment.[23]

B. $\Lambda^0\eta^0$ Final State

There were 16 fits to the reaction $K^-p \to \Lambda^0\eta^0$ ($\eta^0 \to \gamma\gamma$) and zero background events were predicted. Even though there are few events, we have used them to compute a cross section for the $\Lambda^0\eta^0$ final state which could be compared with previous measurements.[8] No cuts were applied to the 16 events, and after weighting, they give cross sections of 0.37 ± 0.13 mb for $0.72 < P_K < 0.76$ GeV/c and 0.16 ± 0.10 mb for $0.76 < P_K < 0.82$ GeV/c in agreement with other measurements.

C. $\Lambda^0\pi^+\pi^-$ and $\Sigma^0\pi^+\pi^-$ Final States

Much previous data exist for the charged-pion final states in our momentum region as the Λ^0 and Σ^0 reactions are easily separable in hydrogen.[3,5,6] For the $\Lambda^0\pi^+\pi^-$ events, we have divided the fits into four momentum bins, weighted for Λ losses and for a double-scanning efficiency determined from the scan data to be 0.90 ± 0.07. The events corrected for the background yield cross sections for the average momentum in each bin which are $\sigma(0.63\ \text{GeV}/c) = 2.20 \pm 0.49$ mb, $\sigma(0.69\ \text{GeV}/c) = 2.66 \pm 0.47$ mb, $\sigma(0.75\ \text{GeV}/c) = 3.08 \pm 0.50$ mb, and $\sigma(0.81\ \text{GeV}/c) = 2.98 \pm 0.73$ mb. These values are plotted in Fig. 13, where we show a comparison between our data points and other experiments. The agreement is good.

As seen in Table IV, the best estimate of the background in the $\Sigma^0\pi^+\pi^-$ (1γ) final state was zero, therefore, no background subtraction was made. The cross sections were computed for two bins of 0.10 GeV/c width from 0.66 to 0.86 GeV/c, yielding values of $\sigma(0.71\ \text{GeV}/c) = 0.75 \pm 0.12$ mb and $\sigma(0.81\ \text{GeV}/c) = 0.77 \pm 0.19$ mb. These results are also plotted in Fig. 13 along with data points from the hydrogen experiments.

D. $\Lambda^0\pi^0$ Final State

The $\Lambda^0\pi^0$ events provided the best final state to check our event weighting and determination of the background. In this momentum region, $\Lambda^0\pi^0$ events can be separated rather cleanly in hydrogen

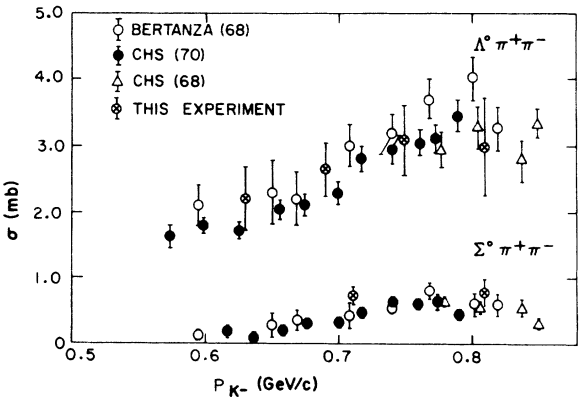

FIG. 13. Measured cross sections for $\Lambda^0\pi^+\pi^-$ and $\Sigma^0\pi^+\pi^-$ as a function of K^- beam momentum.

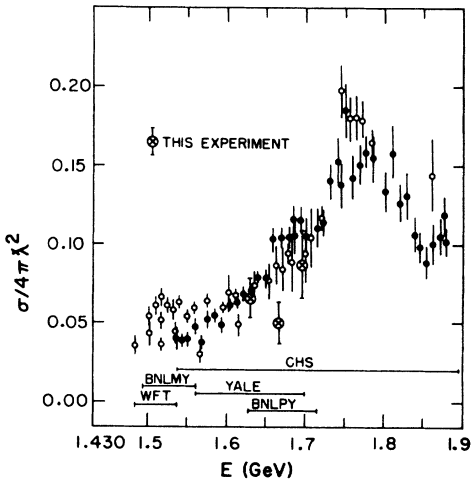

FIG. 14. $\Lambda^0\pi^0$ cross sections as a function of center-of-mass energy.

experiments by looking at the missing mass off the Λ^0. In order to compute cross sections, a correction factor for the events with lost γ due to low projected momentum was determined by application of the empirically determined efficiency function, discussed in Section II D. Our measured cross sections are shown in Fig. 14 and compared to previous hydrogen results. Although our measured cross section for the central energy bin is somewhat lower than the average, our results are statistically compatible with previous experiments.

The center-of-mass angular distributions after background subtraction are plotted in Fig. 15 for the π^0 with respect to the beam direction. The angular distributions are shown in the same three momentum bins for which cross sections were computed. The events plotted are those with χ^2 probability above 0.01. The errors given reflect the uncertainties due to statistics and the assigned event weights. For bins in which there were no events, a statistical error of ± 1 was assigned and weighted by the average weight per event in that momentum region.

In order to compare our distributions with the hydrogen results, we have taken the data from the CHS collaboration[3,6] normalized to our observed flux distribution as determined from the τ decays, and we have summed the results over the corresponding momentum bins to obtain the angular distributions that would correspond to ours. We have then renormalized the CHS data to give the same total cross section as our data. The resulting CHS points are depicted in Fig. 15 as rectangles

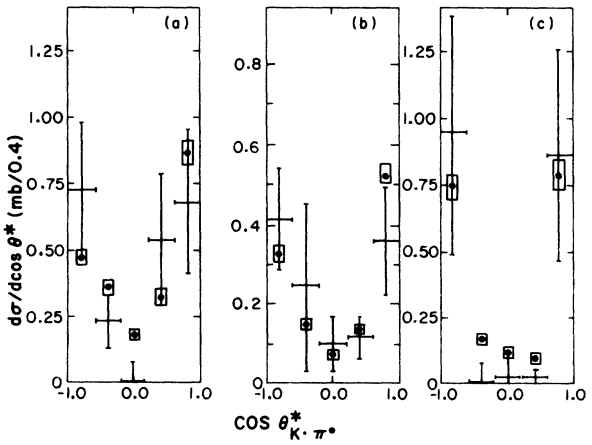

FIG. 15. The $\Lambda^0\pi^0$ center-of-mass angular distributions: (a) $0.62 \leq P_{K^-} \leq 0.70$ GeV/c, (b) $0.70 \leq P_{K^-} \leq 0.78$ GeV/c, and (c) $0.78 \leq P_{K^-} \leq 0.86$ GeV/c. The CHS distributions are shown as rectangles normalized to the area under the histogram. The height of each rectangle represents the CHS errors.

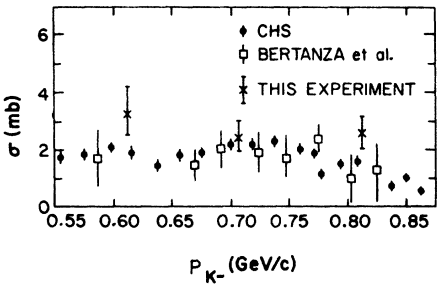

FIG. 16. $\Sigma^0\pi^0$ cross sections as a function of beam momentum for the 2γ and 3γ events.

with height equal to the error calculated from their article. Our angular distributions shown are in good agreement with the CHS data.

E. $\Sigma^0\pi^0$ Final State

In hydrogen experiments, the $\Sigma^0\pi^0$ cross section has been estimated by looking at the missing mass from the Λ^0. In this experiment, we have isolated a sample of $\Sigma^0\pi^0$ events with two and three observed γ rays. For the 2γ events, due to the ambiguity with the $\Lambda^0\pi^0$ final state, only $\Sigma^0\pi^0$ fits that used a measured γ ray in forming the Σ^0 were used. After the χ^2 probability cuts, 3γ and 2γ samples were obtained with backgrounds of 3% and 17%, respectively.

The 2γ events were divided into three bins of 0.10 GeV/c. After subtracting the background events, these gave cross sections of $\sigma(0.61\ \text{GeV}/c) = 5.03 \pm 2.06$ mb, $\sigma(0.71\ \text{GeV}/c) = 2.65 \pm 1.17$ mb, and $\sigma(0.81\ \text{GeV}/c) = 2.99 \pm 1.16$ mb. In a similar fashion, the 3γ events were divided into the same momentum bins and after weighting each event and making a background subtraction, the resulting cross sections are $\sigma(0.61\ \text{GeV}/c) = 2.71 \pm 0.87$ mb,

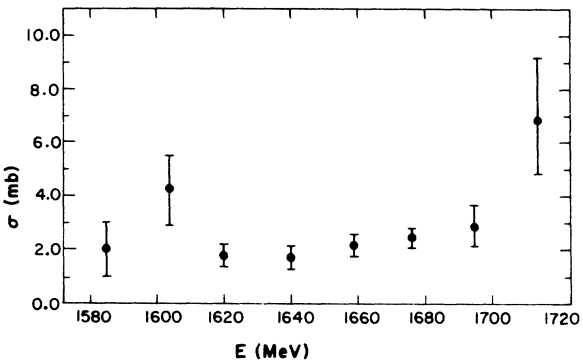

FIG. 17. The $\Sigma^0\pi^0$ cross sections in 20-MeV bins as a function of center-of-mass energy for the 2γ and 3γ events.

$\sigma(0.71\ \text{GeV}/c) = 2.41 \pm 0.56$ mb, and $\sigma(0.81\ \text{GeV}/c) = 2.37 \pm 0.70$ mb.

The 2γ and 3γ cross sections are statistically compatible and give weighted averages of $\sigma(0.61\ \text{GeV}/c) = 3.39 \pm 0.87$ mb, $\sigma(0.71\ \text{GeV}/c) = 2.49 \pm 0.54$ mb, and $\sigma(0.81\ \text{GeV}/c) = 2.60 \pm 0.62$ mb. These are shown in Fig. 16. We have also computed cross sections in 40-MeV/c bins. This corresponds to center-of-mass energy bins of about 20 MeV, which was the computed mass resolution in the experiment. In Fig. 17, we have plotted these cross sections as a function of the center-of-mass energy. No significant structure is revealed at this level of statistics.

In the $\Sigma^0\pi^0$ angular distributions of Fig. 18, we have imposed only the χ^2 probability cut. The distributions are the weighted average of the 2γ and 3γ events and have the background subtracted. The angular distributions are tabulated in Table V. The CHS data were normalized using our observed flux distribution and total cross section and are shown as rectangles with heights representing the errors. CHS angular distributions for the entire momentum range from 0.76 to 0.86 GeV/c are not available. On these same plots, we have also shown the predicted distributions for $\Sigma^0\pi^0$ using the amplitudes derived by Kim in his multichannel phase-shift analysis,[24] which included the CHS data. There are some differences between our distributions and the CHS data. The significance of these differences depends on the relative normalization between the two sets of data. With the normalization shown, a discrepancy appears in the forward direction and in the backward direction, where our results suggest a somewhat sharper distribution.

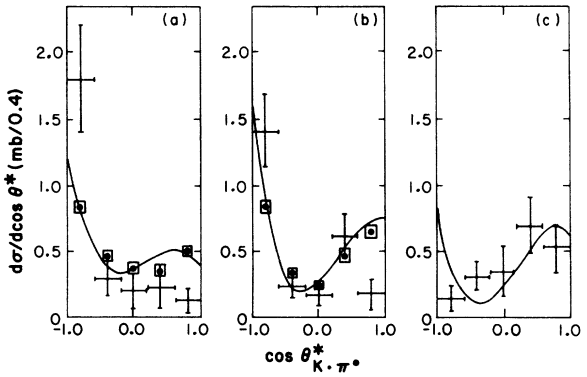

FIG. 18. The $\Sigma^0\pi^0$ (3γ) and $\Sigma^0\pi^0$ (2γ) corrected angular distributions weighted together: (a) $0.62 \leq P_{K^-} \leq 0.70$ GeV/c, (b) $0.70 \leq P_{K^-} \leq 0.78$ GeV/c, and (c) $0.78 \leq P_{K^-} \leq 0.86$ GeV/c. Rectangles are the CHS data as explained in the text. The curves are from Kim's analysis.

TABLE V. $\Sigma^0\pi^0$ center-of-mass angular distributions. The differential cross sections and errors are given in mb/0.4.

P_{K^-} (GeV/c)	0.56–0.66	0.66–0.76	0.76–0.86
(2γ)			
−1.0 to −0.6	1.91± 0.61	1.60± 0.41	1.18± 0.58
−0.6 to −0.2	0.91± 0.63	0.22± 0.11	0.47± 0.20
−0.2 to 0.2	1.95± 1.37	0.20± 0.15	0.41± 0.32
0.2 to 0.6	0.00± 0.18	0.64± 0.22	0.52± 0.21
0.6 to 1.0	0.26± 0.20	0.00± 1.03	0.41± 0.28
(3γ)			
−1.0 to −0.6	1.70± 0.48	1.25± 0.42	0.00± 0.09
−0.6 to −0.2	0.18± 0.13	0.23± 0.10	0.23± 0.14
−0.2 to 0.2	0.10± 0.10	0.15± 0.11	0.30± 0.25
0.2 to 0.6	0.68± 0.37	0.58± 0.24	1.17± 0.55
0.6 to 1.0	0.05± 0.10	0.20± 0.09	0.67± 0.30
($2\gamma + 3\gamma$)[a]			
−1.0 to −0.6	1.80± 0.39	1.40± 0.28	0.16± 0.11
−0.6 to −0.2	0.30± 0.14	0.24± 0.08	0.32± 0.10
−0.2 to 0.2	0.21± 0.12	0.18± 0.10	0.34± 0.20
0.2 to 0.6	0.23± 0.16	0.62± 0.16	0.70± 0.22
0.6 to 1.0	0.14± 0.10	0.18± 0.12	0.54± 0.20

[a]Weighted average of 2γ and 3γ events.

F. $\Lambda^0\pi^0\pi^0$ and $\Sigma^0\pi^0\pi^0$ Final States

In hydrogen experiments, the same analysis which yielded the $\Sigma^0\pi^0$ cross sections also yielded a cross section for the combined $\Lambda^0\pi^0\pi^0$ and $\Sigma^0\pi^0\pi^0$ final states. The four-body production was considered to be small at these energies as evidenced by the $\Lambda^0\pi^+\pi^-\pi^0$ cross sections[5] so that all the events can be considered $\Lambda^0\pi^0\pi^0$ and $\Sigma^0\pi^0\pi^0$.

After making the χ^2 probability cut for the $\Lambda^0\pi^0\pi^0$ (3γ) events, we divided the remaining events into three 0.08-GeV/c momentum bins from 0.62 to 0.86 GeV/c. After weighting each event separately for γ-ray and Λ losses, the background

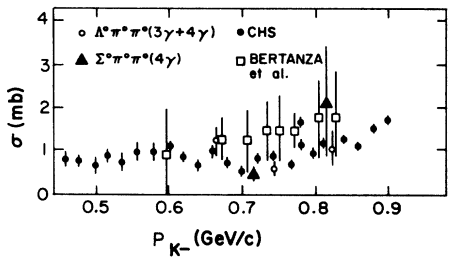

FIG. 19. The three-body final-state cross sections as a function of K^- beam momentum. The $\Lambda^0\pi^0\pi^0$ (4γ) events have been weighted together and plotted as circles. Also shown are the $\Sigma^0\pi^0\pi^0(4\gamma)$ cross sections which are plotted as triangles.

events were subtracted. The cross sections, based on the subtracted events and averaged with the few 4γ events, are $\sigma(0.66\ \mathrm{GeV}/c) = 1.23 \pm 0.33$ mb, $\sigma(0.74\ \mathrm{GeV}/c) = 0.63 \pm 0.16$ mb, and $\sigma(0.82\ \mathrm{GeV}/c) = 1.02 \pm 0.44$ mb. These cross sections are plotted separately in Fig. 19 where the hydrogen data for the combined $\Lambda^0\pi^0\pi^0$ and $\Sigma^0\pi^0\pi^0$ cross sections are also shown for comparison. In Fig. 20(a), we have weighted together the $\Lambda^0\pi^0\pi^0$ (3γ) and $\Lambda^0\pi^0\pi^0$ (4γ) cross sections after subtracting background and plotted them as a function of center-of-mass energy in 20-MeV bins. No significant enhancement is observed near the 1660-MeV region.

The $\Sigma^0\pi^0\pi^0$ (4γ) events were divided into two bins of 0.10-GeV/c width from 0.66 to 0.86 GeV/c. There were 7 and 8 events, respectively, which yielded cross sections of $\sigma(0.71\ \mathrm{GeV}/c) = 0.45 \pm 0.16$ mb and $\sigma(0.81\ \mathrm{GeV}/c) = 2.12 \pm 1.32$ mb. These values are also plotted in Fig. 19. The cross section computed for the three observed $\Sigma^0\pi^0\pi^0$ (5γ) events over a 0.20 GeV/c bin from 0.66 to 0.86 GeV/c was $\sigma(0.76\ \mathrm{GeV}/c) = 1.62 \pm 1.22$ mb. Because of the small 5γ sample, we have restricted our studies of this final state to the 4-γ-ray sample. The $\Sigma^0\pi^0\pi^0$ (4γ) cross sections in 20-MeV bins are shown in Fig. 20(b). In all momentum regions,

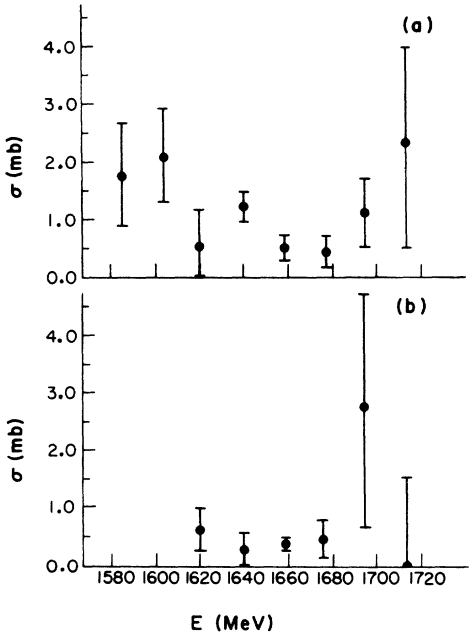

FIG. 20. Plot (a) shows the $\Lambda^0\pi^0\pi^0$ cross sections as a function of center-of-mass energy. The 3γ and 4γ events have been weighted together. Plot (b) shows the $\Sigma^0\pi^0\pi^0$ (4γ) cross section as a function of center-of-mass energy.

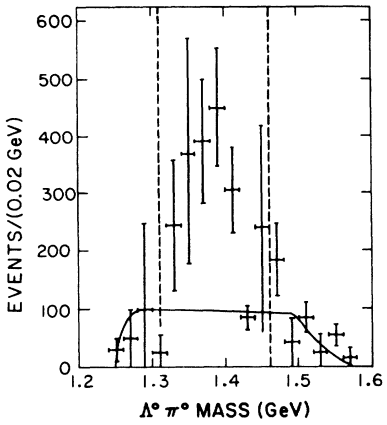

FIG. 21. The $\Lambda^0\pi^0$ mass distributions for the 3γ and 4γ $\Lambda^0\pi^0\pi^0$ events weighted together with two entries per event. The phase-space curve is fitted to the data outside the $\Sigma(1385)$ region, shown by the dashed lines.

we find that combining our cross sections for $\Lambda^0\pi^0\pi^0$ and $\Sigma^0\pi^0\pi^0$ yields answers consistent both with the Bertanza data and the CHS data.

The $\Lambda^0\pi^0$ mass distribution is shown for the 3γ and 4γ $\Lambda^0\pi^0\pi^0$ events in Fig. 21. The plot contains two points per event and the dashed vertical lines show the predicted region containing one full width of the $\Sigma(1385)$ including our resolution. The solid curve is phase-space normalized to the data outside the $\Sigma(1385)$ region. Complications arise in the study of $\Sigma(1385)$ production in this final state due to Bose-Einstein statistics and interference of overlapping bands in the Dalitz plots. Therefore,

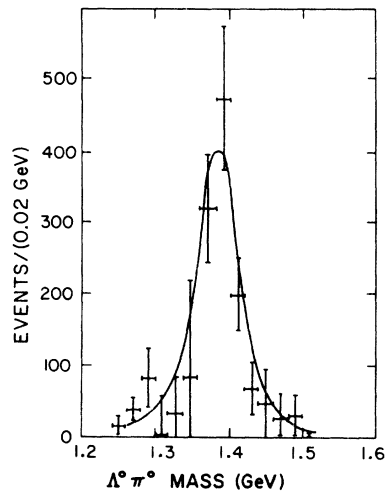

FIG. 22. The $\Lambda^0\pi^0$ mass combination closest to the $\Sigma(1385)$. A Breit-Wigner curve smeared by the mass resolution in this region is shown on the data.

we have adopted the simple approach of plotting in Fig. 22, the $\Lambda^0\pi^0$ mass combination nearest to the $\Sigma(1385)$. A Breit-Wigner curve smeared by the mass resolution has been placed on the data, and it shows a good agreement. Thus, there is evidence for strong $\Sigma(1385)$ production in this final state, consistent with 100% production at the statistical level of this experiment.

To conclude the discussion of the $\Lambda^0\pi^0\pi^0$ events, we have shown in Fig. 23 the $\pi^0\pi^0$ mass-squared distribution versus the center-of-mass angular distributions for the $\pi^0\pi^0$ system for the 4γ events. We can, in principle, observe background that might exist in a $\Sigma^0\pi^0$ final state from the hydrogen experiments if the $\pi^0\pi^0$ direction were misassigned to the meson in the $\Sigma^0\pi^0$ angular distribution. The CHS experiment has plotted the missing mass squared off the Λ^0 and selected events in an interval from 0.04 GeV^2 to 0.20 GeV^2 in order to isolate their $\Sigma^0\pi^0$ signal. This interval in our experiment consists of a $\pi^0\pi^0$ system which goes predominantly forward in the center-of-mass frame. Thus such events may have preferentially contributed to the CHS $\Sigma^0\pi^0$ angular distributions in the foward direction shown in Fig. 18. The 3γ $\Lambda^0\pi^0\pi^0$ events (not shown) reveal the same effect after making a background subtraction.

The $\Sigma^0\pi^0$ mass distribution for the 4γ $\Sigma^0\pi^0\pi^0$ events is shown in Fig. 24. A solid curve shows the phase-space distribution, and the histograms contain two combinations per event. In Fig. 25, the $\Sigma^0\pi^0$ mass combination closest to the $\Lambda(1405)$ is plotted. Each event plotted in Figs. 24 and 25 has an associated weighting factor which accounts for a number of other events which were undetected. The uncertainty in this weighting factor is propagated through, so that an error in a bin represents both the statistical fluctuation in population of

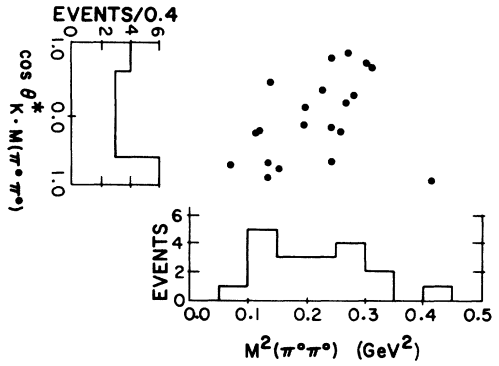

FIG. 23. Cosine of the angle between the $\pi^0\pi^0$ system and the beam direction versus mass squared of the $\pi^0\pi^0$ system.

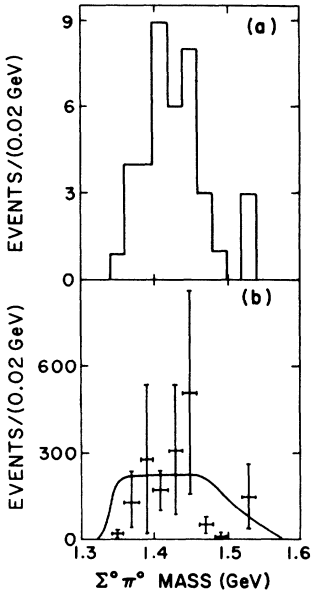

FIG. 24. $\Sigma^0\pi^0$ mass for the $\Sigma^0\pi^0\pi^0$ (4γ) events. The solid curve is phase space. Plot (a) shows unweighted events and plot (b) shows the weighted events.

events in that bin and errors in the weights. The latter are also partly statistical in nature in that the weight assigned to an event depends on the particular kinematic configuration of the γ's and the Λ^0 for that event. For some kinematic configurations, the weights and the error on the weights are both large.

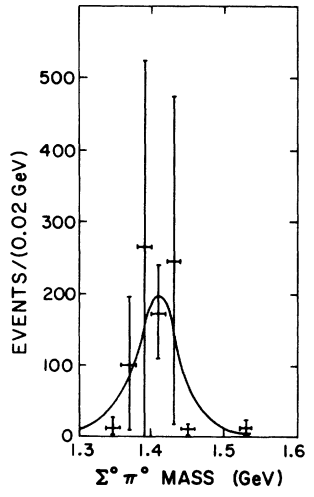

FIG. 25. $\Sigma^0\pi^0$ mass combination nearest the $\Lambda(1405)$ for the $\Sigma^0\pi^0\pi^0$ events. The curve is a Breit-Wigner curve with the natural width of the $\Lambda(1405)$, smeared by the experimental mass resolution.

A Breit-Wigner curve for the $\Lambda(1405)$ smeared by our resolution is also shown in Fig. 25. There is evidence for $\Lambda(1405)$ production, consistent with 100% $\Lambda(1405)$ at the statistical level of this experiment.

V. SUMMARY AND CONCLUSIONS

The heavy-liquid-bubble-chamber technique that was employed in this experiment allows for a study of final states which contain γ rays. The agreement of our results with previous hydrogen data for the $\Lambda^0\pi^+\pi^-$, $\Sigma^0\pi^+\pi^-$, $\Lambda^0\pi^0$, and $\Lambda^0\eta^0$ final states confirms the reliability of our γ-ray techniques and normalization procedures. The total cross section obtained for the final states $\Sigma^0\pi^0$, $\Lambda^0\pi^0\pi^0$, and $\Sigma^0\pi^0\pi^0$ are found to be compatible with existing measurements from previous hydrogen experiments. None of these cross sections show evidence for any significant energy structure at the statistical level of this experiment. The cross sections presented for the $\Sigma^0\pi^0\pi^0$ and $\Lambda^0\pi^0\pi^0$ final states represent the first measurements of these reactions.

The appearance of a small discrepancy with previous hydrogen data in the angular distributions for $\Sigma^0\pi^0$ might be qualitatively explained from possible contamination due to the $\pi^0\pi^0$ final states. Due to the relatively large statistical errors, the $\Sigma^0\pi^0$ data presented here do not in themselves warrant a phase-shift analysis, but rather contribue new information, which should be incorporated into the more general multi-channel phase-shift programs.

The $\Lambda^0\pi^0\pi^0$ and $\Sigma^0\pi^0\pi^0$ final states appear to be dominated by two-body production. The pure $I=0$ state $\Lambda^0\pi^0\pi^0$ results from strong $\Sigma(1385)\pi^0$ production and is consistent with 100% $\Sigma(1385)\pi^0$. The pure $I=1$ state $\Sigma^0\pi^0\pi^0$ shows evidence of strong $\Lambda(1405)\pi^0$ production, and again the data are compatible with 100% $\Lambda(1405)\pi^0$. Since isospin conservation prohibits the decay of $\Sigma(1385)$ into $\Sigma^0\pi^0$, this latter final state is free of any $\Lambda(1405)$ ambiguity with $\Sigma(1385)$.

ACKNOWLEDGMENTS

We are indebted to the valuable support of our programming and scanning staff at ANL, especially Astride Jakobsons, C. Kosner, P. Fiala, S. Watson, M. Umbrasas, P. Orange, and S. Johnson. We are indebted to the Scanning Staff at Concordia. We also wish to thank the 40-in. bubble-chamber crew for their help with the exposure.

---

*Work performed under the auspices of the U. S. Atomic Energy Commission.

†AUA-ANL Predoctoral Fellow. Present address: Imperial College, London, England.

‡Present address: Nuclear Physics Laboratory, Oxford University, Oxford, England.

§Present address: Biomedical Computation Center, University of Chicago, Chicago, Illinois 60637.

[1]R. Armenteros, M. Ferro-Luzzi, D. W. G. S. Leith, R. Levi-Setti, A. Minten, R. D. Tripp, H. Filthuth, V. Hepp, E. Kluge, H. Schneider, R. Barloutaud, P. Granet, J. Meyer, and J. P. Porte, Z. Physik 202, 486 (1967).

[2]R. Armenteros, M. Ferro-Luzzi, D. W. G. S. Leith, R. Levi-Setti, A. Minten, R. D. Tripp, H. Filthuth, V. Hepp, E. Kluge, H. Schneider, R. Barloutaud, P. Granet, J. Meyer, and J. P. Porte, Nucl. Phys. B3, 592 (1967).

[3]R. Armenteros, P. Baillon, C. Bricman, M. Ferro-Luzzi, H. K. Nguyen, V. Pelosi, D. E. Plane, N. Schmitz, E. Burkhardt, H. Filthuth, E. Kluge, H. Oberlack, R. R. Ross, R. Barloutaud, P. Granet, J. Meyer, J. L. Narjoux, F. Pierre, J. P. Porte, and J. Prevost, Nucl. Phys. B8, 216 (1968).

[4]J. H. Bartley, R. Y. L. Chu, R. M. Dowd, A. F. Greene, J. Schneps, W. H. Sims, J. R. Albright, E. B. Brucker, J. E. Lannutti, B. G. Reynolds, M. Meer, J. E. Mueller, M. Schneeberger, and S. E. Wolf, Phys. Rev. Letters 21, 1111 (1968).

[5]L. Bertanza, A. Bigi, R. Carrara, R. Casali, R. Pazzi, D. Berley, E. L. Hart, D. C. Rahm, W. J. Willis, S. S. Yamamoto, and N. S. Wong, Phys. Rev. 177, 2037 (1968).

[6]R. Armenteros, P. Baillon, C. Bricman, F. Ferro-Luzzi, E. Pagiola, J. O. Peterson, D. E. Plane, N. Schmitz, E. Burkhardt, H. Filthuth, E. Kluge, H. Oberlack, R. R. Ross, R. Barloutaud, P. Granet, J. Meyer, J. P. Porte, and J. Prevost, Nucl. Phys. B21, 15 (1970).

[7]W. C. Harrison, Ph.D. thesis, Florida State University, 1970 (unpublished).

[8]M. E. Binkley, D. W. Carpenter, B. B. Cox, L. R. Fortney, E. C. Fowler, C. M. Rose, and W. M. Smith, preliminary report, Department of Physics, Duke University, 1970 (unpublished).

[9]D. Sinclair, in *Proceedings of the Twelfth International Conference on High Energy Physics, Dubna, 1964* (Atomizdat, Moscow, 1966), Vol. II, p. 478 (translation).

[10]G. Keyes, M. Derrick, T. Fields, L. G. Hyman, J. G. Fetkovich, J. McKenzie, B. Riley, and I. T. Wang, Phys. Rev. D 1, 66 (1970).

[11]More details about this experiment may be found in T. Dombeck, Ph.D. thesis, Northwestern Univ., 1972 (unpublished); ANL/HEP Report No. 7213, 1972 (unpublished).

[12]C. T. Murphy, University of Michigan Bubble Chamber Group research note 65/67, 1967 (unpublished).

[13]A. Lagarrigue and A. Rousset, in *Bubble and Spark*

Chambers, edited by R. P. Shutt (Academic, New York, 1967), Vol. I, p. 159.
[14]S. Praestein, ANL/HEP Report No. 7140, 1971 (unpublished).
[15]R. Bock, CERN Report No. DD/EXP/62/10, 1962 (unpublished).
[16]Particle Data Group, Rev. Mod. Phys. 43, S1 (1971).
[17]W. Heitler, *The Quantum Theory of Radiation* (Clarendon, London, 1957).
[18]J. W. Motz, H. A. Olsen, and H. W. Koch, Rev. Mod. Phys. 41, 581 (1969).
[19]H. A. Bethe and J. Ashkin, in *Experimental Nuclear Physics*, edited by E. Segrè (Wiley, New York, 1960), Vol. I, p. 328.
[20]G. Bozoki, E. Fenyves, T. Gemesy, E. Gombosi, S. Krasznovszky, E. Nagy, N. P. Bogachev, Yu. A. Budagov, V. B. Vinogradov, A. G. Volodko, V. P. Dzhelepov, V. G. Ivanov, V. S. Kladnitsky, S. V. Klimenko, Yu. F. Lomakin, Yu. P. Merekov, I. Patočka, V. B. Fliagin, and P. V. Shlyapnikov, Phys. Letters 28B, 360 (1968).
[21]M. E. Binkley, D. W. Carpenter, J. R. Elliot, L. R. Fortney, E. C. Fowler, J. P. Golson, J. E. Kronenfeld, C. M. Rose, T. R. Snow, and W. M. Yeager, Phys. Rev. D 4, 3250 (1971).
[22]Tai Ho Tan, Phys. Rev. Letters 23, 102 (1969).
[23]C. Mayeur, P. Van Binst, G. Wilquet, V. B. Fliagine, J. G. Guy, W. L. Knight, S. N. Tovey, R. M. Dowd, M. Govan, A. J. Sanders, J. Schneps, and G. Wolsky, Phys. Letters 33B, 441 (1970).
[24]Jae Kwan Kim, Phys. Rev. Letters 27, 356 (1971).

PHYSICAL REVIEW D VOLUME 7, NUMBER 5 1 MARCH 1973

Final States with Three Charged Particles and a Visible Λ from K^-d Interactions at 4.5 GeV/c*

A. C. Ammann,† D. D. Carmony, A. F. Garfinkel, L. J. Gutay, and D. H. Miller
Physics Department, Purdue University, Lafayette, Indiana 47907

and

W. L. Yen
Physics Department, Indiana University-Purdue University at Indianapolis, Indianapolis, Indiana 46205
(Received 2 June 1972)

This report concerns itself with the study of four- or five-body final states produced by the interaction of 4.48-GeV/c K^- mesons on neutrons. The data result from a 372 000-picture exposure in the Argonne National Laboratory 30-in. deuterium-filled bubble chamber. The reactions studied include (1) $K^-n \to \Lambda\pi^+\pi^-\pi^-$, (2) $K^-n \to \Sigma^0\pi^+\pi^-\pi^-$, (3) $K^-n \to \Lambda\pi^+\pi^-\pi^-\pi^0$, (4) $K^-n \to \Lambda\pi^+\pi^-\pi^-$MM, (5) $K^-n \to \Lambda\pi^-K^+K^-$, and (6) $K^-n \to \Lambda\pi^-K^0_LK^0_S$, where all the Λ particles decayed visibly. Evidence is presented for the existence of the $\Sigma(1640)$ whose mass and width are 1642 ± 12 MeV/c^2 and 55 ± 24 MeV/c^2, respectively. The branching ratios are found to be consistent with an octet assignment. The A_2 data are presented and are compatible with $J^{PC} = 2^{++}$. In addition, the productions of ρ^0, ω, and ϕ^0 are discussed in conjunction with simultaneous $\Sigma^-(1385)$ production and the results are compared with quark-model predictions.

I. INTRODUCTION

The primary purpose of this experiment was to study the interaction of K^- mesons with neutrons. To this end, 372 000 exposures were made at the deuterium-filled MURA 30-in. bubble chamber at Argonne National Laboratory using a 4.48-GeV/c K^- beam. Almost all the data analyzed here consist of four- and five-particle final states containing a visible Λ decay. Four- and five-particle final states containing a visible $\overline{K}^0$ decay[1] and two- and three-particle final states containing a visible neutral decay[2,3] have been studied elsewhere.

Analysis of the data is divided into three sections. The existence and branching ratios of hyperon resonances in the 1.6-GeV/c^2 mass region is investigated under the topic of baryon resonances. Included under meson resonances is a study of the controversial A_2 region of the three-pion mass spectrum. The angular distributions and cross sections of the quasi-two-body reactions resulting in baryon–vector-meson resonance production are compared with predictions of the quark model in the last section.

II. EXPERIMENTAL DETAILS

The film was scanned for events of the types three- or four-prong plus vee and one- or two-prong plus two vees. In the case of even-prong events it was demanded that one of the positive particles (the spectator) had a range of less than 15 cm. All events of these topologies were mea-